International Journal of Engineering

Journal Homepage: www.ije.ir

Effect of Deformation-Induced Defects on the Microstructure and Pitting Corrosion Behavior of Al-Ag Alloy

P. Afzali, M. Yousefpour*, E. Borhani

Faculty of Materials and Metallurgical Engineering, Semnan University, Semnan, Iran

P A P E R I N F O

Paper history:
Received 21 July 2018
Received in revised 28 September 2018
Accepted 26 October 2018

Keywords:
Corrosion
Pitting
Al-Ag
Cold Work Deformation
Precipitation

A B S T R A C T

In this study, a wide range of combined ageing treatments and cold work deformations in the Al 4.2 wt% Ag alloy matrix were proposed, aiming to investigate the effect of defects such as precipitates (Ag_2Al plates) and dislocations on the mechanical and electrochemical behavior of Al–4.2 wt% Ag alloys. Further reductions of thickness from 10 to 60%, decreases the mean size of Ag_2Al plates, along with a denser distribution. The inductive loop at lower frequencies in Nyquist plot attributed to localized corrosion that clearly testified the fluctuations of the anodic branch in the Tafel diagram and the FE-SEM images for the presence of pitting corrosion. Additionally, the pit propagation grade expands repetitively with cold work reduction and fragmentation of pre-precipitates. This was related to an extreme amount of dislocations induced by deformation and fragmented pre-precipitates, which created more preferable locations for the nucleation of pits. Furthermore, Energy Dispersive X-ray Spectroscopy of pits, revealed that the presence of Al-Ag containing particles acted as cathodic sites and caused the anodic matrix dissolution.

***doi**: 10.5829/ije.2018.31.12c.14*

1. INTRODUCTION

Al-Ag alloys are widely used in electrical devices such as electrical conductors and superconductors. This is due to considerable electrical conductivity they can generate at applied temperatures. Creating the opportunity to obtain a conductor with a higher current capacity. Due to high price of silver, the need for conducting more experiments on this alloy by the industries in order to avoid time-consuming and expensive trials and failures is of great importance [1]. The silver/metal oxide which forms on the surface of these alloys can easily increase the electrical resistance of the conductor; hence, the corrosion behavior of these alloys must be investigated in detail. Before using Al-Ag alloys as electrical contacts such a wires or plates, the Al-Ag alloy is pre-deformed for improved mechanical strength [2]. Additionally, some aluminum alloys such as Al-Ag and Al-Cu are prone to age hardening treatment, by this process intermetallic precipitates will appear in their microstructure. The most significant feature of precipitation hardening would be the increase of hardness. These precipitates can be considered as catalytic sites for corrosion and pit nucleation in the matrix. Previous investigations into the microstructure and different heat treatments of Al-Ag alloys have facilitated a wide understanding in the sequence and temperature of producing the precipitates [3-7]. The other preferred sites of microstructure for corrosion are dislocations, which are mainly created by mechanical work. Many past research on the effect of cold work on corrosion behavior of different alloys has been carried out [8-13]. The effect of cold work on pitting corrosion of 00Cr18Mn15Mo2N0.86 stainless showed that the localized corrosion of the specimen was generally unaltered with increases of cold deformation up to 50% [14]. An effort was made by Wan et al. [11] on corrosion behavior of pre-deformed 2219 Al alloy, in which a greater amount of pre-deformation caused an increase in dislocation density and more θ′ phases start the nucleation process which degraded the pitting

*Corresponding Author Email: *myousefpor@semnan.ac.ir* (M. yousefpour)

Please cite this article as: P. Afzali, M. Yousefpour, E. Borhani. Effect of Deformation-Induced Defects on the Microstructure and Pitting Corrosion Behavior of Al-Ag Alloy, International Journal of Engineering (IJE), IJE TRANSACTIONS C: Aspects Vol. 31, No. 12, (December 2018) 2092-2101

corrosion resistance. A research [15] revealed that the localized corrosion of 7xxx series aluminum alloys on account of the age hardening process and creation of precipitates led to the galvanic contact between $Al7Cu_2Fe$ and the matrix correspondingly altered, which affected the vulnerability to localized corrosion. This was contributed to the fainter galvanic series between Al_3Fe particles and the matrix. The effect of intermetallic defects on the localized corrosion behavior of AA2099-T83 aluminum-lithium alloy has been investigated [1]. It was found that various amounts of copper in Al-Fe-Mn-Cu-(Li) resulted in pitting corrosion of the alloy. Additionally, the increase of lithium established more active sites than the low-copper-containing particles. Electrochemical impedance spectroscopy measurements (EIS) including nyquist, bode and phase angle plots are used in corrosion measurements of aluminum and its alloys. The pre-deformation effect on corrosion of 2024-T4 aluminum alloy was investigated by Chen et al. [16] and indicated that pre-deformation can change the micro-structure of a material, increasing the corrosion driving force, as well as anodic dissolution rate. Due to the potential difference between the treated zone and the matrix, the amount of Mg can greatly affect the electrochemical behavior of Al–Cu–Mg–Ag alloy [17]. In a project the effect of mechanical loading on the galvanic corrosion behavior of a magnesium-steel structural joint was investigated [18]. The applied forces were found to increase the localized corrosion around the galvanic joints. The experiment [19, 20] also evaluated the impact of water immersion parameters according to the temperature and pH on trivalent chromium conversion coatings and corrosion factors formed on AA2024-T351 alloy. Some corrosion protection properties were investigated in different media and coatings. The inhomogeneity of the surface was a reason for potential difference which causes the localized corrosion. This clarifies that both micro-structure defects (precipitate as intermetallic particles and dislocation which are respectively created by age hardening and cold work) can play an important role on corrosion, specifically on pitting corrosion of aluminum alloys [8, 10, 21-23]. In regard to electrochemical corrosion, little is known about the unique electrochemical corrosion of Al-Ag alloy. Besides, Al-Ag is susceptible to pitting corrosion. Particularly when the alloy has second phase particles and dislocations in its micro-structure so that these particles are preferred sites for corroding [2]. Besides, there are not numerous researches on the characterization of corrosion behavior of Al-Ag [24, 25]. For Al-Ag alloys, some microstructural researches have been done as discussed in the aforementioned references, but the corrosion behavior, specifically the effect of cold work on pitting corrosion has not been widely evaluated. Therefore, it should be interesting to determine how the interaction of cold working process and ageing treatment can affect the corrosion behavior of Al-Ag.in this paper, initially, the microstructure was studied, then the corrosion behavior was determined by potentiodynamic polarization and electrochemical impedance spectroscopy (EIS) methods.

2. MATERIALS AND METHODS

2. 1. Material Preparation and Microstructural Investigations An aluminum-silver (Al– 4.2 wt% Ag) alloy was used in this research. The specimens, were cut into 15 mm × 15 mm × 3 mm plates, solution-treated at 540 °C for 2 hours in an air furnace, then quenched in water immediately. In order to make sure that all specimens were micro-structurally similar, solid solution heat treatment (SSHT) was carried out to dissolve probable pre-formed coarse precipitates in the matrix. The sheet was cut into four plates, three of these were aged at 200 °C and the forth at 270 °C for 8 hours. Subsequently, the aged specimens were prepared for the hardness measurements which were executed by MMT7-Buchler Micro-Vickers hardness tester. Vickers hardness of the aged specimens measured with a loading bar and time of 0.98 N and 10s, respectively, at seven different positions for each specimen and eventually the mean hardness value was estimated from the values except for the maximum and minimum measures which were out of range.

A rolling machine was used to perform the work hardening process by reducing the specimens' thickness to obtain different desired reduction percentage. The 200 °C aged specimens were cold rolled to a 10, 20 or 60% reduction in thickness (denoted as 200-10%, 200-20%, 200-60% respectively) and the 270 °C age specimen was cold rolled to 60% reduction in thickness (270-60% specimen was tested in order to verify and perceive the effect of higher temperature variations of this specimen in comparison to 200-60% specimen since both include the same amount of reduction but different ageing temperatures).

Afterwards, the hardness of all cold rolled specimens were measured again. The specimens were ground with SiC abrasive papers to 3000 grit, polished with Al_2O_3 paste to achieve a smooth surface. This was followed by surface cleaning.

Subsequently, the micro-structures of all specimens was characterized by FE-SEM and the crystalline phase structure was determined by Bruker D8 Advance X-ray diffraction (XRD; Bruker Corporation, Karlsruhe, Germany). Dislocation density and crystallite size were evaluated using Williamson-Hall (WH) method, in accordance with the data obtained from XRD test.

2. 2. Electrochemical Investigations To prepare working electrodes of the electrochemical tests, the specimens were sealed with an epoxy resin to expose an area of $1cm^2$. The corrosion tests were carried out with a three-electrode electrochemical cell setup in a 3.5% NaCl solution at room temperature. The solution of 3.5% NaCl in double distilled was prepared by dissolving the appropriate mass of NaCl. A platinum (Pt) sheet was used as the counter electrode, a silver/silver chloride (Ag/AgCl) was served as the reference electrode. The stable open circuit potential period before both potentiodynamic polarization and EIS experiments were determined at 45 min. Potentiodynamic polarization measurements were performed by a scanning rate of 0.1 mV/s (by ASTM G59 / G5) with potential range from -1.3 to -0.3 V, then the OCP was recorded. Afterwards, EIS was performed with potential amplitude of 10 mV (rms) over the frequency range of 10^4 Hz to1 Hz. Finally, each specimen was cleaned with acetone, alcohol, then rinsed gently with deionized water, dried, and stored in a desiccator. In order to study the surface morphology and pitting mechanism, field emission scanning electron microscope and energy dispersive spectroscopy (SEM-EDS) were used.

3. RRESULTS AND DISCUSSIONS

3. 1. Effect of Precipitates and Cold Work on Hardness Value of Al-4.2 wt% Ag The main reason of any increase in hardness is the rigorous movement of dislocations. The dislocations may move through the lattice structure or may be cut by the other defects. As seen in Figure 1, the mean Vickers hardness values for aged specimens without deformation (200, 270) are reported as 50 and 41 Hv, respectively. This reduction of hardness (throgh the increase of ageing temperature from 200 to 270 °C) might be due to coarsening of precipitates which reached to over-aged temperature. These coarse particles lessened efficient pinning and bounding interaction of defects (precipitates and some dislocations which are made during aging process) due to comfortable movements of dislocation. As a result, the mean micro hardness value of the aged 270 °C specimen (without deformation) turned into lower values [26]. Figure 1 also indicates that the increase of cold work from 10 to 60% for the 200 °C specimen, increased the hardness value. In addition, the 270-60% specimen has the highest hardness value due to its greater ageing temperature and the highest amount of cold work. This illustrates that cold work treatment has significant influence on hardness, due to the produced dislocations and fragmentation of precipitates. Therefore, the interaction between dislocations and precipitates leads to increase of hardness [27-29]. Considering the hardness values of the 270 °C specimen with and without deformation (66 and 46, respectively), it is evident that regardless of, the coarsening of Ag_2Al precipitates during ageing process has reduced the hardness amount, but the 60% deformation on the same specimen (270 °C without deformation) has increased the hardness significantly, as if its value reached maximum. It is concluded that the interaction of over aged precipitates and dislocations in Al-Ag matrix can significantly increase the hardness.

3. 2. FESEM Observations of Precipitates The discrepancy of atomic numbers of Al and Ag elements makes an appropriate high-contrast for FE-SEM image and an ideal pattern model for microstructural investigations [30]. FE-SEM images of all deformed specimens are presented in Figure 2.

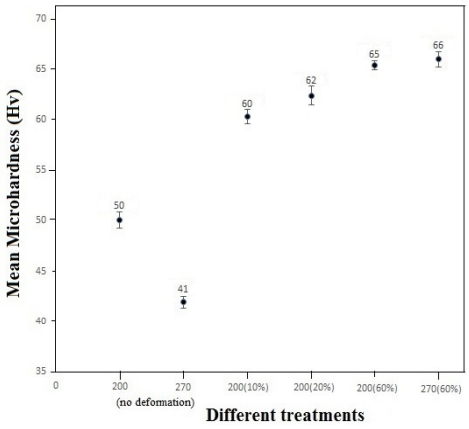

Figure 1. Vickers micro-hardness of Al–4.2 wt% Ag alloy specimens after different cold working

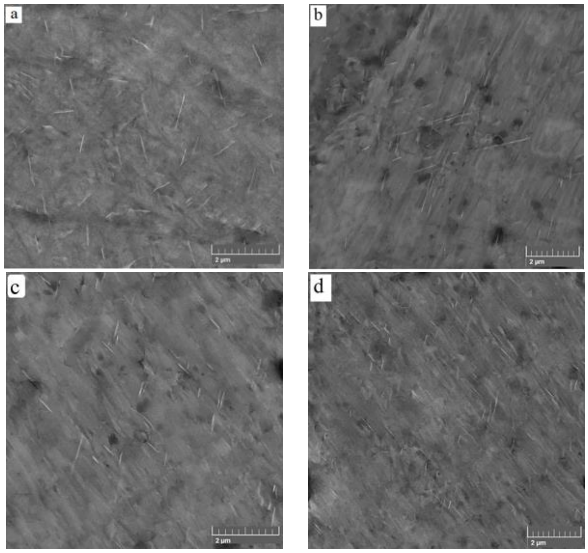

Figure 2. FE-SEM images of Al–4.2 wt% Ag alloy: a: 200(10%), b: 200(20%), c: 200(60%) and d: 270(60%)

The uniform and homogeneous distribution of precipitation has formed in the Al matrix of all specimens. The needle like plates of Ag_2Al precipitates is clearly observed in Al (α) matrix. Additionally, the FE-SEM images in Figure 2 visually illustrate that by increased amount of cold work, the precipitates are fragmented and shortened in length.

3. 3. Phase Analysis, Islocation Density and Crystallite Size by Williamson-Hall (WH) Method

The transformation of phase composition for various deformations and heat treatments are shown in diffraction patterns in Figure 3.

Figure 3, indicates there are two diffraction peaks at the scattering angles of 36.00°, 41.13° for all specimen and can be assigned to the (100) and (101) planes of the Ag_2Al crystal lattice, respectively [31]. X-ray diffraction (XRD) was used to measure the dislocation density and crystallite size (grain size).

The obtained data were analyzed using the Williamson-Hall (WH) method. In this method, β, is the broadening of the hkl diffraction peak measured at half of its maximum intensity (in radians) which is related to the lattice strain, ε, by the Equation (1) [29]:

$$(\beta \frac{\cos \emptyset}{\lambda} = \frac{0.9}{D} + \varepsilon \frac{2 \sin \emptyset}{\lambda}) \quad (1)$$

where, θ, λ, and D are the diffraction angle, X-ray wavelength, and crystallite size, respectively. The β for each (hkl) peak is obtained by plotting the value of β $\frac{\cos \emptyset}{\lambda}$ as a function of $\frac{2 \sin \emptyset}{\lambda}$. The lattice deformation stress and crystallite size were, extracted from the slope and intersection of the y-axis. The dislocation density, ρ, was derived from the Equation (2), [29].

$$\rho = 14.4\left(\frac{\varepsilon}{b}\right)^2 \quad (2)$$

where b is the magnitude of the Burgers vector. The calculated value of the dislocation density and crystallite size of all specimens are shown in Figure 4.

It is important to relate the mechanical properties of the age-deformed specimens containing pre-existing precipitates to the structural parameters, such as dislocation density, grain size of the matrix and the size of the precipitates. Figure 4. indicates that the dislocation density and crystallite size are in a reverse relationship as if with the increase of dislocation density the crystallite size decreases. Furthermore, the dislocation density increased with an increase of deformation; this result positively correlates with the preceding discussion on hardness measurement earlier [32]. One possible reason for the grain-refinement acceleration in 200(60%) and 270(60%) specimens could be their high dislocation density and influence of the pre-existing precipitates on dislocation motion during plastic deformation.

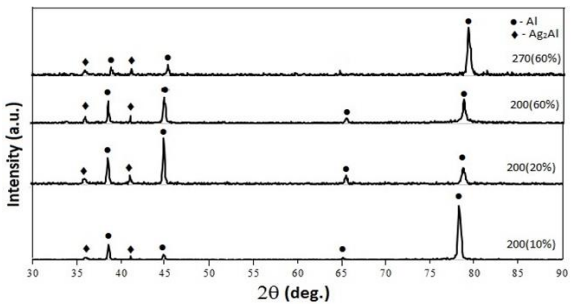

Figure 3. X-ray diffraction pattern of the Al–4.2 wt% Ag specimens

3. 4. Potentiodynamic Polrization Measurements

Figure 5 illustrates the potentiodynamic polarization curves of the Al–4.2 wt% Ag alloys processed at different amount of deformation.

The corrosion current density and corrosion potential for all specimens was determined with the Tafel extrapolation method. The anodic polarization curve is the most important feature related to the corrosion resistance behavior [33-37]. According to the mixed-potential theory, the corrosion potential (Ecorr)

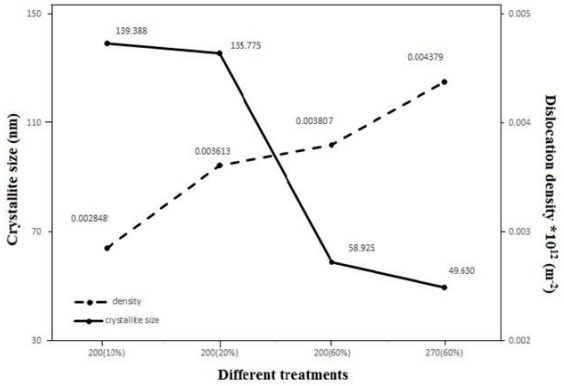

Figure 4. The calculated value of the dislocation density and crystallite size of different cold working

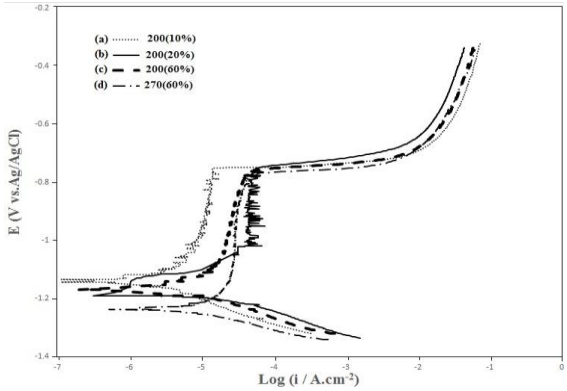

Figure 5. Potentiodynamic polarization curves: a: 200(10%), b: 200(20%), c: 200(60%) and d: 270(60%)

as a thermodynamic parameter must be assessed by extrapolation of the both anodic and cathodic branches. Implying that any amount of increase in cathodic current density will result in a change in corrosion potential of the anodic branch. Although an increase of the anodic current density would cause a shift of the corrosion potential in the cathodic branch, due to the presence of a passive film on Al and its alloys, a more negative value of corrosion potential (Ecorr), is often related to more active pits that would lead to a higher corrosion tendency [38, 39].

Table 1 shows the values of the corrosion potential (Ecorr), current density (Icorr) and pitting potential (Epit). Table 1 demonstrates that the 200(10%) specimen has the least corrosion current density (5.24807×10^{-7} A/cm^2) as well as the noblest corrosion and pitting potentials (-1.142, -0.7499 VAg/AgCl, respectively). The corrosion current density for 200(20%) deformed specimen increased to 1.23026×10^{-6} A/cm^2 as well as corrosion and pitting potentials (-1.151 and -0.751 VAg/AgCl, respectively) are close to the corrosion and pitting potentials parameters for the 200(10%) specimen. A greater amount of cold work deformation indicates that the 200(60%) specimen including corrosion current density of 1.90546×10^{-6} A/cm^2 and the corrosion and pitting potentials of -1.175, -0.759 VAg/AgCl, respectively have more susceptible conditions for occurrence of corrosion. Finally the 270(60%) specimen which has different ageing temperature but the same deformation percentage compared to 200(60%) specimen, is analyzed and it is indicated that the 270(60%) specimen has the most corrosion current density (5.01187 × 10-6 A/cm^2), with the highest negative values for corrosion and pitting potentials (-1.234, -0.772 VAg/AgCl, respectively). Pitting corrosion is considered to be affected by the attendance of secondary phases and defects like precipitates, dislocations and constituents. It is important to note that the number, size and distribution of precipitates are influential in destructive behavior of pitting corrosion [40, 41]. On that account, it can be concluded that an increase of cold work deformation level has obviously deteriorated the corrosion resistance of all specimens and degraded the pitting potential to more negative values.

TABLE 1. Corrosion parameters obtained from Potentiodynamic polarization test for Al–4.2 wt% Ag specimens (a) 200(10%), (b) 200(20%), (c) 200(60%), (d) 270(60%)

Level of cold work	i_{corr} (A/cm^2)	E_{corr} (VAg/AgCl)	E_{pit} (VAg/AgCl)
(a) 200(10%)	5.24807×10^{-7}	-1.142	-0.749
(b) 200(20%)	1.23026×10^{-6}	-1.151	-0.751
(c) 200(60%)	1.90546×10^{-6}	-1.175	-0.759
(d) 270(60%)	5.01187×10^{-6}	-1.234	-0.772

There would be several reasons to attribute the decrease of corrosion resistance to the deformation. One could be the presence of micro defect such as: dislocations, second phase precipitates and grain boundaries [42-44]. The mechanism of how these defects affect the corrosion resistance is that they create localized micro galvanic series. Hence, with an increase of corrosion current density and stored energy, more electric current will travel across the surface, increasing the driving force of the oxidation reactions on the surface. The metal ions would also move from these preferred sites onto the surface, towards the solution [40, 45]. Furthermore, these pre-existing precipitates and dislocations (induced by precipitation hardening and cold work deformation, respectively) can also be favorable locations for the nucleation of pits [46-48] Considering the aforementioned mechanisms, this paper indicates that with increase of cold work all the Al–4.2 wt% Ag specimens decrease in their corrosion and pitting potentials and an increase in the corrosion current densities. As a result, with further reduction in thickness (10% to 60%), the corrosion resistance decreased due to the increase of dislocation density and fragmentation of long precipitates to finer pieces, causing the precipitates to increase in number and these more defects can cause more favorable site for pit nucleation. In addition, further decrease of corrosion resistance in the 270(60%) specimen in comparison with 200(60%) specimen might be due to the drastic increase of ageing temperature to the 70 °C which could have led to further coarsen precipitates being created.

3. 5. Electrochemical Impedance Spectroscopy (EIS) Impedance measurements are greatly used as a reliable method to inquire into not only the mechanisms and behavior of uniform corrosion but also the localized corrosion. The clarification of electric elements application, needs suitable elucidation of obtained impedance results [46, 49]. EIS data was analyzed with ZsimpWin (EchemSoftware, Princeton Applied Research) using electrical equivalent circuit models. To achieve an optimum fitting result, relative estimated errors of the calculated parameters by the software, the errors were kept at a minimum percentage and the best fitting results were reported. Figure 6 shows impedance plots ((a). Nyquist, (b). bode, (c). phase angle) of deformed specimens.

EIS diagrams for cold worked specimens show similar features. All the Nyquist plots (Figure 6a) show a small depressed capacitive semicircle at higher frequencies, related to the thin fragile pre-formed passive oxide layer on the metal (which can be seen in a magnified square in the down-left side of the Figure 6a).

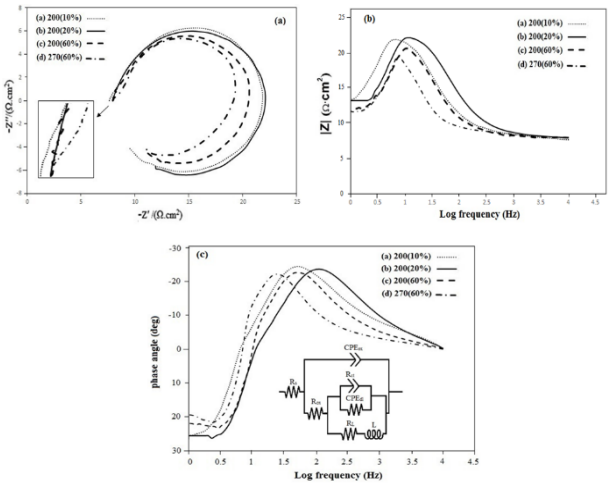

Figure 6. EIS spectra presented as impedance plot: a: Nyquist, b: Bode and c: Phase angle and the electrochemical equivalent circuits for EIS fitting for all specimens

A second large capacitive loop at intermediate frequencies is attributed to corrosion procedure on metal surface, followed by an inductive loop at lower frequencies attributed to localized corrosion. The presence of the inductive loop is examined repeatedly in order to ensure that the inductive loop is not an artifact of the testing process. The equivalent circuit is used for modelling the EIS, results are shown in the Figure 6c. The extracted parameters according to the model are presented in Table 2. The physical basis for the circuit model used for impedance fitting is as follows, Rs is solution resistance, CPE_{ox} and R_{ox} represent a constant phase element and a thin fragile pre-made passive oxide layer resistance respectively, CPE_{dl} and R_{ct} are constant phase elements of the double layer capacitance. The charge transfer resistance respectively and L, R_L are attributed to the inductance and inductance resistance. It is demonstrated in bode plots (Figure 6b) that the impedance values do not vary in the frequency range of 103–104 Hz which shows the solution resistance. Due to further increase of deformation amount, the bode-phase plot for all specimens shows a drop-in impedance of all frequencies (Figure 6b). Figure 6c shows the phase maxima at intermediate frequencies. Assigning presence of time constant controlling the charging/discharging of electrical double layer and low frequencies (around 10 HZ), which assigns the presence of time constant, attributed to the thin fragile pre-made passive oxide layer on the metal.

Frequency width of the maximum phase angle 24◦ (Figure 6c) decreases by an increase of cold work deformation amount from 10 to 60%, illustrating the degradation of corrosion resistance. Constant phase element (CPE) has been introduced to imitate the electrochemical behavior of an imperfect capacitor. CPE is described by two parameters Y and n according to the equation [50, 51]:

$$Z_{CPE}(Y, n) = \frac{1}{Y(J\omega)^n} \quad (3)$$

where, Y is the CPE-constant, j the imaginary unit, n the CPE power ($0 \le n \le 1$), and ω is the angular frequency.

$$\omega = 2\pi f \quad (4)$$

For n=1 the CPE is a pure capacitance. For a capacitance element the deviation of the exponent n from unity is due to the heterogeneousness effect. CPE (Y, n) in Table 2, represents the constant phase element for the large capacitive loop at intermediate frequencies attributed to the corrosion procedure on metal surface; where Y and n are the parameters of the CPE. The capacitance of double layer (C_{dl}) was calculated from the following formula:

$$C_{dl} = Y^{\frac{1}{n}} Rct^{\frac{1-n}{n}} \quad (5)$$

where, R is the double layer resistance (R_{ct}) [52-54]. Electrochemical impedance data which is obtained from the equivalent circuit model fitting has been calculated and embedded in the circuit model in order to achieve the most accurate and reliable impedance data.

Also, the value alterations of the above electrochemical impedance data are directly in a logical relation to each other. For instance, all the resistance parameters in Table 2, such as thin fragile pre-made passive oxide layer resistance (R_{ox}), the charge transfer resistance (R_{ct}) and inductance resistance (R_L) are all increasing in all specimens with further amount of deformation. The quantitative results have been obtained by fitting the EIS data and are collected in Table 2.

TABLE 2. Impedance parameters deduced from the analysis of impedance spectra for cold worked specimens

Level of cold work	R_{ox} (Ω cm^2)	$Y_{ox} \times 10^{-4}$ (Ω^{-1} cm^{-2} S^n)	n_{ox}	R_{ct} (Ω cm^2)	$Y_{dl} \times 10^{-4}$ (Ω^{-1} cm^{-2} S^n)	n_{dl}	C_{dl} (mF cm^{-2})	R_L (Ω cm^2)	L (H)
(a) 200(10%)	1.872	5.91	0.93	14.15	2.820	0.84	0.104	12.35	0.93
(b) 200(20%)	1.759	4.85	0.83	14.13	1.966	0.91	0.109	10.17	0.56
(c) 200(60%)	1.693	6.18	0.85	12.61	3.776	0.94	0.275	9.36	0.52
(d) 270(60%)	1.403	2.83	0.96	11.34	10.100	0.95	0.831	8.37	0.39

The table indicates that the charge transfer resistance (R_{ct}) and R_{ox} of both capacitive loops are decreased by a greater amount of cold work process and the capacitance of double layer (C_{dl}) is increased. The value of resistance parameters as well as of the capacitance of double layer for 200(10%) and 200(20%) specimens are close together due to their close amount of cold work.

3. 6. FE-SEM and EDS Analysis Specimens of different deformation and different heat treatment were subjected to FE-SEM observation and Pitting morphology after potentiodynamic polarization tests are observed in Figure 7. The micrographs confirm that the pitting corrosion damage on the surfaces of all specimens is obvious and the severity of pitting attacks is enhanced by the increase in cold work amount. All the pitting corrosion morphologies of deformed specimens include various kind of pits, considering number, size, shape, depth and distribution.

All of these features are likely to have a direct relationship with the number, size, shape, distribution and the interaction of the pre-made micro-structural defects such as precipitations and dislocation. Thus, intermetallic particles and defects could influence the pitting corrosion behavior as a second phase. It is indicated that further cold work increases the number of pits. Seemingly, the 200(60%) and 270(60%) specimens have more widespread pitting attack which seems to be distributed along the surface to a greater extent. Additionally, the pits in 200(10%) and 200(20%) specimens appear to be short and small in number, indicating that the corrosion is not so severe.

The EDX composition analysis spectra of pit and matrix zones in Figure 7c, are presented in Figure 8. The EDX spectrum (a) of the Al-Ag matrix, free from precipitates represents O, Al, Ag and Si peaks. Suggesting that these observations are comprehensively consistence to electrochemical data and particularly to corrosion current density. This pitting process is due to strong galvanic coupling between defects (High dislocations density, precipitates) and matrix.

The presence of oxygen contributes to the anodic passive oxide layer formation on the surface. The low Si content seems to be the impurity.in addition, the presence of Ag indicates that a small amount of silver remained in the Al matrix as a solid solution. As shown in Figure 8b the EDX analysis shows the Al an Ag peaks indicating the presence of Ag and Al inside the pitting area as Ag_2Al intermetallic precipitates. Hence, during the electrochemical procedure on the surface, the precipitates did not dissolve, and the pitting corrosion occurred around the Ag_2Al plates on the Al matrix. From FE-SEM/EDS analysis it is determined that the bright intact intermetallics are close to the pitting areas in Figure 7.

Therefore, Ag_2Al precipitates act as cathodic sites in the Al-Ag alloy and the selective dissolution occurs at the Al matrix, acting as an anodic site.

The result of surface observations can prove that the electrochemical results and the difference in the degree of pitting attacks on the surface led to a better understanding of the effect of deformation process on corrosion.

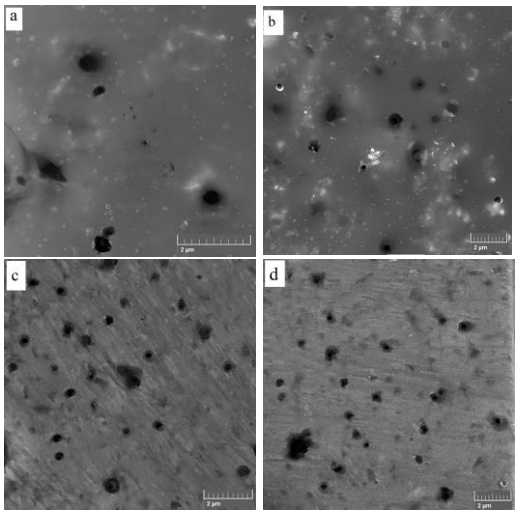

Figure 7. Pitting corrosion morphologies of deformed specimens (a) 200(10%), (b) 200(20%), (c) 200(60%) and (d) 270(60%)

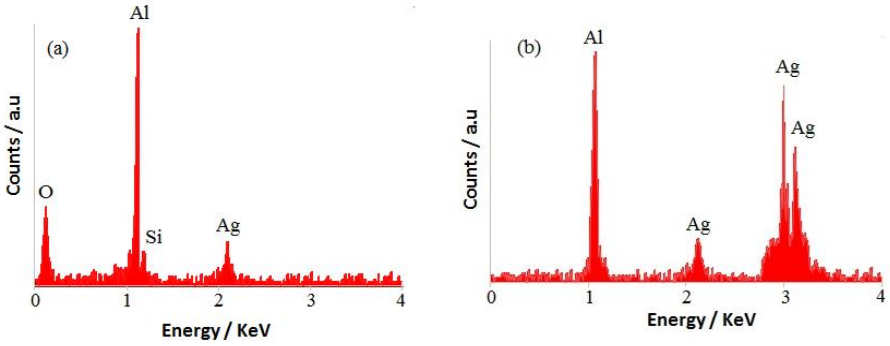

Figure 8. EDX spectra of Al–4.2 wt% Ag alloy (200(60%)) specimen. (a) matrix, (b) pit

4. CONCLISION

1. An increase of deformation percentage from 10 to 60%, increased the hardness values. In addition, the 270(10%) specimen had a greater hardness value in comparison to the 200(60%) specimen. This is likely due to its greater ageing temperature, which had reached to peak aged temperature. Also, in the case of the hardness values of the 270 °C specimen with and without deformation, it is obvious that even though, the coarsening of Ag_2Al precipitates during ageing process reduced the hardness amount, the 60 percent deformation on the same specimen increased the hardness significantly, as if its value reached maximum.
2. Potentiodynamic measurements, revealed that with increase an of cold work, all specimens showed a decrease in their corrosion and pitting potentials and an increase in the corrosion current densities as a result of more defects, which led to a higher stored energy and created more local galvanic cells, thus increasing the electron activity. Furthermore, the greater decrease of corrosion resistance in the 270(60%) specimen in comparison to the 200(60%) specimen could be due to a drastic increase of ageing temperature to the 70 °C which leads to creating more coarsened precipitates. The pit propagation grade expands repetitively with cold work reduction. This was related to an extreme amount of dislocations induced by the deformation and fragmented precipitates, which created more preferable locations for the nucleation of pits
3. From an electrochemical perspective, EIS measurements showed that charge transfer resistance (R_{ct}) and R_{ox} of two capacitive loops decreased by further amount of cold work process and the capacitance of double layer (C_{dl}) increased; indicating the degradation of corrosion resistance by further amount of cold work.
4. EDS analysis showed that the pitting corrosion occurred around the Ag_2Al plates on the anodic dissolved the Al matrix and precipitates acted as cathodic.

5. ACKNOWLEDGMENT

The authors would like to appreciate the assistance provided by the research board of Semnan University for the provision of the research facilities for this project.

6. REFERENCES

1. Mamala, A., Knych, T., Kwaśniewski, P., Kawecki, A., Kiesiewicz, G., Sieja-Smaga, E., Śc Iężor, W., Gniełczyk, M., and Kowal, R., "New Al-Ag Alloys for Electrical Conductors with Increased Current Carrying Capacity", ***Archives of Metallurgy and Materials***, Vol. 61, No. 4, (2016), 1875–1880.
2. He, Q., Yang, H., Chen, L., Fan, X., Shen, Q., Wu, X., Mu, C., and Zhang, L., "Study on the Mechanical Alloying Process for Preparing Ag/LSCO Electrical Contact Material", ***Procedia Engineering***, Vol. 94, (2014), 37–43.
3. Afzali, P., Yousefpour, M., and Borhani, E., "Evaluation of the effect of ageing heat treatment on corrosion resistance of Al–Ag alloy using electrochemical methods", ***Journal of Materials Research***, Vol. 31, No. 16, (2016), 2457–2464.
4. Pang, M., Zhan, Y., Yang, W., Li, C., Wang, H., Jiang, W., and Du, Y., "First-principles calculations on the crystal, electronic structures and elastic properties of Ag-rich γ′ phase approximates in Al–Ag alloys", ***Computational Materials Science***, Vol. 51, No. 1, (2012), 415–421.
5. Erni, R., Heinrich, H., and Kostorz, G., "High-resolution Z-contrast STEM of Guinier–Preston zones in Al–3 at.% Ag", ***Materials Chemistry and Physics***, Vol. 81, No. 2–3, (2003), 227–229.
6. Nicholson, R.B., and Nutting, J., "The metallography of precipitation in an Al-16% Ag alloy", ***Acta metallurgica***, Vol. 9, No. 4, (1961), 332–343.
7. Talha, M., Behera, C.K., and Sinha, O.P., "In-vitro long term and electrochemical corrosion resistance of cold deformed nitrogen containing austenitic stainless steels in simulated body fluid", ***Materials Science and Engineering: C***, Vol. 40, (2014), 455–466.
8. Jinlong, L., Hongyun, L., tongxiang, L., and wenli, G., "The effects of grain refinement and deformation on corrosion resistance of passive film formed on the surface of 304 stainless steels", ***Materials Research Bulletin***, Vol. 70, (2015), 896–907.
9. Ghosh, S., and Kain, V., "Effect of surface machining and cold working on the ambient temperature chloride stress corrosion cracking susceptibility of AISI 304L stainless steel", ***Materials Science and Engineering: A***, Vol. 527, No. 3, (2010), 679–683.
10. Tsao, L.C., Chen, C.H., Wu, R.W., Chang, S.Y., and Chen, R.S., "Plastic flow behavior, microstructure, and corrosion behavior of AZ61 Mg alloy during hot compression deformation", ***Journal of Manufacturing Processes***, Vol. 18, (2015), 167–174.
11. Wan, M., Zhao, Y., Zeng, W., and Cai, G., "Effects of cold pre-deformation on aging behavior and mechanical properties of Ti-1300 alloy", ***Journal of Alloys and Compounds***, Vol. 619, (2015), 383–388.
12. Naeini, M.F., Shariat, M.H., and Eizadjou, M., "On the chloride-induced pitting of ultra fine grains 5052 aluminum alloy produced by accumulative roll bonding process", ***Journal of Alloys and Compounds***, Vol. 509, No. 14, (2011), 4696–4700.
13. Ren, Y., Zhao, H., Liu, W., and Yang, K., "Effect of cold deformation on pitting corrosion of 00Cr18Mn15Mo2N0.86 stainless steel for coronary stent application", ***Materials Science and Engineering: C***, Vol. 60, (2016), 293–297.
14. Wang, S.-S., Huang, I.-W., Yang, L., Jiang, J.-T., Chen, J.-F., Dai, S.-L., Seidman, D.N., Frankel, G.S., and Zhen, L., "Effect of Cu Content and Aging Conditions on Pitting Corrosion Damage of 7xxx Series Aluminum Alloys", ***Journal of The Electrochemical Society***, Vol. 162, No. 4, (2015), C150–C160.
15. Ma, Y., Zhou, X., Huang, W., Thompson, G.E., Zhang, X., Luo, C., and Sun, Z., "Localized corrosion in AA2099-T83 aluminum–lithium alloy: The role of intermetallic particles", ***Materials Chemistry and Physics***, Vol. 161, (2015), 201–210.
16. Chen, Y., Zhou, J., Liu, C., and Wang, F., "Effect of pre-deformation on the pre-corrosion multiaxial fatigue behaviors of 2024-T4 aluminum alloy", ***International Journal of Fatigue***, Vol. 108, (2018), 35–46.

17. Liu, X.Y., Wang, Z.P., Fu, B.G., Long, L., Zhang, X.L., and Cui, H.X., "Effects of Mg content on the mechanical properties and corrosion resistance of Al–Cu–Mg–Ag alloy", ***Journal of Alloys and Compounds***, Vol. 685, (2016), 209–215.
18. Feng, Z., and Frankel, G.S., "Evaluation of Coated Al Alloy Using the Breakpoint Frequency Method", ***Electrochimica Acta***, Vol. 187, (2016), 605–615.
19. Qi, J., Hashimoto, T., Thompson, G.E., and Carr, J., "Influence of Water Immersion Post-Treatment Parameters on Trivalent Chromium Conversion Coatings Formed on AA2024-T351 Alloy", ***Journal of The Electrochemical Society***, Vol. 163, No. 5, (2016), C131–C138.
20. Zamanzade, M., and Barnoush, A., "Effect of chromium on the electrochemical properties of iron aluminide intermetallics", ***Corrosion Science***, Vol. 78, (2014), 223–232.
21. Örnek, C., and Engelberg, D.L., "SKPFM measured Volta potential correlated with strain localisation in microstructure to understand corrosion susceptibility of cold-rolled grade 2205 duplex stainless steel", ***Corrosion Science***, Vol. 99, (2015), 164–171.
22. Dejun, K., and Jinchun, W., "Salt spray corrosion and electrochemical corrosion properties of anodic oxide film on 7475 aluminum alloy", ***Journal of Alloys and Compounds***, Vol. 632, (2015), 286–290.
23. Li, S., Li, Y., Zhang, Y., Liu, J., and Yu, M., "Effect of intermetallic phases on the anodic oxidation and corrosion of 5A06 aluminum alloy", ***International Journal of Minerals, Metallurgy, and Materials***, Vol. 22, No. 2, (2015), 167–174.
24. Riveros, V., Gulppi, M., Páez, M., et al., "Influence of surface treatments in the initial stages of anodizing Al–Ag alloys in neutral electrolytes", ***Journal of Solid State Electrochemistry***, Vol. 10, No. 2, (2006), 83–90.
25. Paez, M., Sandoval, A., Sepulveda, Y., Monsalve, A., Skeldon, P., Thompson, G.E., and Zhou, X., "Anodic oxidation of Al-Ag alloys", ***Corrosion Science***, Vol. 44, No. 12, (1961), 2857–2863.
26. Hossain, A., and Kurny, A.S.W., "Effect of Ageing Temperature on the Mechanical Properties of Al-6Si-0.5Mg Cast Alloys with Cu Additions Treated by T6 Heat Treatment", ***Universal Journal of Materials Science***, Vol. 1, No. 1, (2013), 1–5.
27. Wang, Y., Gupta, R.K., Sukiman, N.L., Zhang, R., Davies, C.H.J., and Birbilis, N., "Influence of alloyed Nd content on the corrosion of an Al–5Mg alloy", ***Corrosion Science***, Vol. 73, (2013), 181–187.
28. Shojaei, K., Sajadifar, S.V., and Yapici, G.G., "On the mechanical behavior of cold deformed aluminum 7075 alloy at elevated temperatures", ***Materials Science and Engineering: A***, Vol. 670, (2016), 81–89.
29. Borhani, E., "Microstructure and Mechanical Property of Heavily Deformed Al-Sc Alloy Having Different Starting Microstructures", Doctoral dissertation, Kyoto University, Japan, (2012).
30. Finkenstadt, D., "Mechanism for Gamma-precipitation in Al-Ag Alloys and Self-assembly of Polyelectrolytes: Modeling of Complex Layered Materials" Doctoral dissertation, University of Illinois at Urbana-Champaign, USA, (2005).
31. Chen, S., Li, X., Niu, G., YI, Z., Chen, Y., Luo, J.-S., Tang, Y.-J., and Sun, W.-G., "Synthesis and characterization of single-phase nanocrystalline Ag2Al particles", ***Transactions of Nonferrous Metals Society of China***, Vol. 22, No. 1, (2012), 134–138.
33. Gubicza, J., Szépvölgyi, J., Mohai, I., Zsoldos, L., and Ungár, T., "Particle size distribution and dislocation density determined by high resolution X-ray diffraction in nanocrystalline silicon nitride powders", ***Materials Science & Engineering A***, Vol. 280, No. 2, (2000), 263–269.
33. Xu, Z., He, L., Tang, Z., Mu, R., and Cao, X., "Evolution of high temperature corrosion behavior of La2(Zr0.7Ce0.3)2O7 with the addition of Y2O3 thermal barrier coatings in contacts with vanadate–sulfate salts", ***Journal of Alloys and Compounds***, Vol. 536, (2012), 106–112.
34. Davó, B., and de Damborenea, J.J., "Use of rare earth salts as electrochemical corrosion inhibitors for an Al–Li–Cu (8090) alloy in 3.56% NaCl", ***Electrochimica Acta***, Vol. 49, No. 27, (2004), 4957–4965.
35. Mishra, A.K., and Balasubramaniam, R., "Corrosion inhibition of aluminum alloy AA 2014 by rare earth chlorides", ***Corrosion Science***, Vol. 49, No. 3, (2007), 1027–1044.
36. Yan CW, He G, X.Y., "The electrochemical research of hot-dip aluminizing film corrosion resistance in seawater", ***Mater Prot***, Vol. 34, (2001), 20–21.
37. Mohammadi, F., and Luo, J., "Effect of cold work on erosion–corrosion of 304 stainless steel", ***Corrosion Science***, Vol. 53, No. 2, (2011), 549–556.
38. Fu, Y., Wu, X., Han, E.-H., Ke, W., Yang, K., and Jiang, Z., "Effects of cold work and sensitization treatment on the corrosion resistance of high nitrogen stainless steel in chloride solutions", ***Electrochimica Acta***, Vol. 54, No. 5, (2009), 1618–1629.
39. Moayed, M.H., Abbaspour, Z., and Sadegian, M.H., "Study of Pitting Corrosion Inhibition of Mild Steel by Nitrite in Concrete Pore Solution by Polarization and Zero Resistance Ammetery (ZRA) Techniques (RESEARCH NOTE)", ***International Journal of Engineering - Transactions B: Applications***, Vol. 22, No. 4, (2009), 369–380.
40. Sun, R., Sun, Q., Xie, Y., Dong, P., Chen, Q., and Chen, K., "Enhancing corrosion resistance of 7150 Al alloy using novel three-step aging process", ***Transactions of Nonferrous Metals Society of China***, Vol. 26, No. 5, (2016), 1201–1210.
41. Ralston, K.D., Birbilis, N., Cavanaugh, M.K., Weyland, M., Muddle, B.C., and Marceau, R.K.W., "Role of nanostructure in pitting of Al–Cu–Mg alloys", ***Electrochimica Acta***, Vol. 55, No. 27, (2010), 7834–7842.
42. Gupta, R.K., Deschamps, A., Cavanaugh, M.K., Lynch, S.P., and Birbilis, N., "Relating the Early Evolution of Microstructure with the Electrochemical Response and Mechanical Performance of a Cu-Rich and Cu-Lean 7xxx Aluminum Alloy", ***Journal of The Electrochemical Society***, Vol. 159, No. 11, (2012), C492–C502.
43. Al-Duheisat, S.A., and El-Amoush, A.S., "Effect of deformation conditions on the corrosion behavior of the low alloy structural steel girders", ***Materials & Design***, Vol. 89, , (2016), 342–347.
44. Xie, D., Wan, G., Maitz, M.F., Sun, H., and Huang, N., "Deformation and corrosion behaviors of Ti–O film deposited 316L stainless steel by plasma immersion ion implantation and deposition", ***Surface and Coatings Technology***, Vol. 214, (2013), 117–123.
45. Hou, Y., Li, Y., Zhang, C., Koizumi, Y., and Chiba, A., "Effects of cold working on corrosion resistance of Co-modified Ni–16Cr–15Mo alloy in hydrofluoric acid solution", ***Corrosion Science***, Vol. 89, (2014), 258–267.
46. Ebrahimi, N., Momeni, M., Kosari, A., Zakeri, M., and Moayed, M.H., "A comparative study of critical pitting temperature (CPT) of stainless steels by electrochemical impedance spectroscopy (EIS), potentiodynamic and potentiostatic techniques", ***Corrosion Science***, Vol. 59, (2012), 96–102.
47. Doolabi, D.S., Ehteshamzadeh, M., and Zarch, M.A., "Microstructure and Corrosion Performance of Silica Coatings on Aluminum Surface Prepared by Plasma Electrolysis Technique", ***International Journal of Engineering*** -

Transactions B: Applications, Vol. 22, No. 3, (2009), 291–298.

48. Hashemi, T., Moztarzadeh, F., and Avanessian, J., "The Potentiodynamic Behavior of Copper in NaCI Solutions Studied by Auger and Photoelectron Spectroscopy", ***International Journal of Engineering***, Vol. 1, No. 1, , 1–6.
49. Afrasiabi, H.A., Khayati, G.R., and Ehteshamzadeh, M., "Studying of Heat Treatment Influence on Corrosion Behavior of AA6061-T6 by Taguchi Method", ***International Journal of Engineering - Transactions C: Aspects***, Vol. 27, No. 9, (2014), 1423–1430.
50. Reuvers, N.J.W., Huinink, H.P., Adan, O.C.G., Garcia, S.J., and Mol, J.M.C., "Water uptake in thin nylon 6 films as measured by electrochemical impedance spectroscopy and magnetic resonance imaging", ***Electrochimica Acta***, Vol. 94, (2013), 219–228.
51. Ryl, J., Wysocka, J., Jarzynka, M., Zielinski, A., Orlikowski, J., and Darowicki, K., "Effect of native air-formed oxidation on the corrosion behavior of AA 7075 aluminum alloys", ***Corrosion Science***, Vol. 87, (2014), 150–155.
52. Seifzadeh, D., and Golmoghani-Ebrahimi, E., "Formation of novel and crack free nanocomposites based on sol gel process for corrosion protection of copper", ***Surface and Coatings Technology***, Vol. 210, (2012), 103–112.
53. Habazaki, H., Kataoka, F., Shahzad, K., Tsuji, E., Aoki, Y., Nagata, S., Skeldon, P., and Thompson, G.E., "Growth of barrier-type anodic films on magnesium in ethylene glycol electrolytes containing fluoride and water", ***Electrochimica Acta***, Vol. 179, (2015), 402–410.
54. Hosseini, M.G., Bagheri, R., and Najjar, R., "Electropolymerization of polypyrrole and polypyrrole-ZnO nanocomposites on mild steel and its corrosion protection performance", ***Journal of Applied Polymer Science***, Vol. 121, No. 6, (2011), 3159–3166.

Effect of Deformation-Induced Defects on the Microstructure and Pitting Corrosion Behavior of Al-Ag Alloy

P. Afzali, M. Yousefpour, E. Borhani

Faculty of Materials and Metallurgical Engineering, Semnan University, Semnan, Iran

P A P E R I N F O

Paper history:
Received 21 July 2018
Received in revised 28 September 2018
Accepted 26 October 2018

Keywords:
Corrosion
Pitting
Al-Ag
Cold Work Deformation
Precipitation

چکیده

در این مطالعه، طیف وسیعی از عملیات پیرسختی و تغییر شکل کار سرد بر روی ماتریکس زمینه آلیاژ Al 4.2 wt% Ag به منظور بررسی تاثیر عیوب از قبیل: رسوبات Ag_2Al و نابجایی‌ها بر رفتار مکانیکی و الکتروشیمیایی آلیاژ مذکور انجام شد. کاهش ضخامت از ۱۰ تا ٦۰ درصد موجب کاهش میانگین اندازه ذرات رسوبی و توزیع چگالتر نابجایی‌ها می‌شود. حلقه‌ی القایی مربوط به فرکانس‌های پایین در نمودار نایکوییست مرتبط با خوردگی موضعی بوده که نوسانات شاخه‌ی آندی در نمودار تافل و تصاویر FE-SEM برای حضور خوردگی موضعی را ثابت می‌کنند. همچنین، میزان گسترش حفرات با کاهش بیشتر ضخامت و خرد شدن رسوبات رابطه مستقیمی دارد. این امر به دلیل میزان بالای نابجایی‌های تشکیل‌شده توسط تغییر شکل و خرد شدن رسوبات است که منجر به تشکیل سایت‌های مناسب برای جوانه‌زنی حفرات می‌شود. به علاوه، طیف‌نگاری EDS از حفرات، نشان داد که حضور ذرات شامل آلومینوم و نقره، به عنوان سایت‌های آندی و کاتدی عمل کرده و موجب انحلال و خوردگی زمینه آندی می‌شود.

***doi**: 10.5829/ije.2018.31.12c.14*